Biomimetic catalysis of nitrite reductase enzyme using copper complexes in chemical and electrochemical reduction of nitrite

Millena P Ferreira, Caio B Castro, João Honorato, Sheng He, Walber Gonçalves Guimarães Júnior, Charlène Esmieu, Eduardo E Castellano, André F de Moura, Daniela R Truzzi, Otaciro R Nascimento, et al.

Biomimetic catalysis of nitrite reductase enzyme using copper complexes in chemical and electrochemical reduction of nitrite

Millena P. Ferreira[a], Caio B. Castro[a], João Honorato [b,c], Sheng He [e], Walber Gonçalves Guimarães Júnior[a], Charlene Esmieu[d], Eduardo E. Castellano[c], André F. de Moura[a], Daniela R. Truzzi[b], Otaciro R. Nascimento[c], Antoine Simonneau[d], Caterina G.C. Marques Netto*[a,e]

Copper nitrite reductase mimetics were synthesized using three new tridentate ligands sharing the same N,N,N motif of coordination. The ligands were based on *L*-proline modifications, attaching a pyridine and a triazole to the pyrrolidine ring, and differ by a pendant group (R = phenyl, *n*-butyl and *n*-propan-1-ol). All complexes coordinate nitrite, as evidenced by cyclic voltammetry, UV-Vis, FTIR and electron paramagnetic resonance (EPR) spectroscopies. The coordination mode of nitrite was assigned by FTIR and EPR as κ^2O chelate mode. Upon acidification, EPR experiments indicated a shift from chelate to monodentate κ*O* mode, and and ^{15}N NMR experiments of a Zn^{2+} analogue, suggested that the related Cu(II) nitrous acid complex may be reasonably stable in solution, but in equilibrium with free HONO under non catalytic conditions. Reduction of nitrite to NO was performed both chemically and electrocatalytically, observing the highest catalytic activities for the complex with *n*-propan-1-ol as pendant group. These results support the hypothesis that a hydrogen bond moiety in the secondary coordination sphere may aid the protonation step.

Introduction

Nitrite (NO_2^-) is formed during the biological oxidation of ammonia or the reduction of nitrate, being one of the intermediates of the biological nitrogen cycle.[1] The metastability of nitrite in biological conditions is related to its action as a hypoxic buffer to assist and maintain vasodilation and mitochondrial respiration due to the formation of nitric oxide (NO) under hypoxia.[2] Therefore, owing to the role of NO as a signaling molecule in vasodilatation, neurotransmission[3] and the need for the removal of nitrogen oxide pollutants from the environment,[4] it is of fundamental interest to develop methods for nitrite reduction to NO.[5-10]

The natural route of nitrite reduction to NO relies on the action of nitrite reductase (NiR) enzymes, which can be classified as class I or class II depending on their active sites. For instance, class I NiR are copper-based (CuNiRs), whereas class II NiRs are multi haem (iron-based) enzymes.[11] CuNiRs assemble cupredoxin-like domains around an active site containing both type 1 (T1Cu) and type 2 Cu (T2Cu). The T1Cu site is responsible for electron transfer to T2Cu, whereas the latter is devoted to nitrite coordination and reduction. In the resting-state, the T2Cu catalytic center is found in the +II oxidation state and exhibits a distorted tetrahedral geometry in a primary coordination sphere composed of three histidine residues and one water molecule[12]. During catalysis, summarized in equation (1), nitrite binds to the T2Cu site after water displacement forming a Cu^{II}-NO_2 intermediate (Fig.1) [13, 14] and after a proton-coupled reduction of Cu^{II}-bound nitrite (NO_2^-), nitric oxide is evolved generating a Cu-OH species[14].

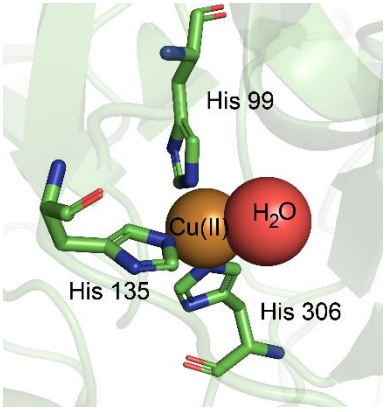

Fig. 1 Active site of CuNiR from from *Achromobacter cycloclastes* (PDB: 2BW4). The T2Cu center has three histidine residues coordinated to the copper. Water is found in the fourth coordination site.

$$Cu^+ + NO_2^- + 2H^+ \rightarrow Cu^{2+} + NO + H_2O \quad (1)$$

Although the exact enzyme mechanism for nitrite reduction is yet to be discovered, there is support for the formation of a copper (II) nitrosyl prior to NO evolution, [15-17] which was recently reported as a stable nitrosyl intermediate with "side-on" binding.[18] However, Cu(II)-nitrosyl might not be formed in all nitrite reductase enzymes. An interesting feature of CuNiR was recently reported by Rose *et al.,* who described that during the enzyme turnover, an aspartate adopts the gatekeeper and proximal positions, controlling substrate passage and guiding the proton transfer step, pointing to new design principles for bio-inspired and bio-mimetic chemical systems.[18]

Several biomimetic complexes of CuNiRs have been described in the literature and the coordination of NO_2^- anions in these models were reported with three different coordination modes: κ^1N (M–NO_2),[19 20] κ^1O (M–ONO)[21] and κ^2O [20 21], but apparently, there is only a minor difference in redox chemistry between the κ^1N and κ^1O isomers.[21] In the related transformation of NO reductive coupling to N_2O, acidic H-bonding functionalities in the secondary coordination sphere were shown to assist the protonation of a putative hyponitrite

[a.] *Department of Chemistry, Universidade Federal de São Carlos (UFSCar), Rod. Washington Luiz, km 235 s/n, CEP 13565905 São Carlos, SP-Brazil, *caterina@ufscar.br*
[b.] *Insitututo de Química, Departanento de Bioquímica, Universidade de São Paulo (USP), Av.Prof.Dr. Lineu Prestes, 748, CEP 05513-970 São Paulo, SP-Brazil*
[c.] *Instituto de Física, Universidade de São Paulo (USP), Av.João Dagnone, 1100, CEP13563-120, São Carlos, SP-Brazil*
[d.] *LCC-CNRS, Universite de Toulouse, CNRS, UPS, 205 route de Narbonne, F31077 Toulouse cedex 4-France*
[e.] *Department of Chemistry, Emory University, 1515 Dickey Drive, 30322 Atlanta,GA-USA*
Electronic Supplementary Information (ESI) available: [details of any supplementary information available should be included here]. See DOI: 10.1039/x0xx00000x

intermediate, efficiently coupling $NO^{\bullet}_{(g)}$ for $N_2O_{(g)}$ production[22] while in heterogeneous NO_2^- hydrogenation, water-bound protons were shown to be responsible for triggering the electron transfer from the catalyst, leading to surface HNO and HNOH species.[23] Interestingly, Cioncoloni *et al.*[20] reported high k_{cat}/K_M values for a complex bearing a carboxylic acid moiety that assists the proton-coupled electron transfer step. More recently, the protonation of a remote site of a copper complex was also shown to be involved in the proton-coupled electron transfer pathway.[9] However, these two examples are based on κ^4N tetracoordinated copper complexes, exhibiting a different geometry than the one found for the copper ion in CuNiRs. In this article, we have designed three copper(II) complexes with a κ^3N coordination environment[24], in which the ligands differ by their secondary coordination spheres. The synthesis, characterization and catalytic activity of these complexes are described, and from these data we could evidence the positive influence of a hydrogen-bonding moiety in the second coordination sphere.

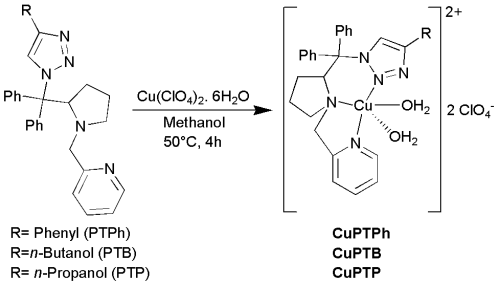

Scheme 1 Synthesis of complexes [CuPTPh] $^{2+}$, [CuPTB] $^{2+}$ and [CuPTP]$^{2+}$.

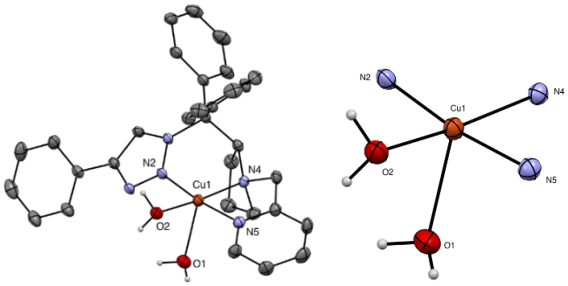

Fig. 2 Molecular structure of **[CuPTPh]$^{2+}$** in the crystal (left) and focus on the distorted square-pyramidal environment of the copper ion (right). Ellipsoids are drawn at the 30% probability level and protons except those of bound water as well as counterions are omitted for clarity

Results

Characterization of the copper complexes

The ligands were designed to obtain a κ^3N coordinative environment around the metallic center. All three ligands derive from a proline-triazole molecule varying by the substituent on the triazole ring (R = phenyl, *n*-butyl and *n*-propan-1-ol). Therefore, they were named accordingly: PTPh (R = phenyl), PTB (R = *n*-butyl) and PTP (R = *n*-propanol), as shown in Scheme 1. The synthetic procedures and characterization of the ligands can be found in the supporting information (Figs. S1-S14). Complexes **[CuPTPh]$^{2+}$**, **[CuPTB]$^{2+}$** and **[CuPTP]$^{2+}$** (Scheme 1) were obtained in high yields (≅90%) and were characterized by microanalysis, EPR, FTIR, high-resolution mass spectroscopy, conductivity, electronic spectroscopy, and cyclic voltammetry (Fig. S15-S21). Complex **[CuPTPh]$^{2+}$** crystallized in methanol, and single crystal X-Ray diffraction (sc-XRD) analysis showed a five-coordinated environment, with a distorted square-pyramidal geometry (Fig. 2), with two water molecules acting as ligands.

FTIR spectroscopy of these complexes also evidences the presence of lattice and coordinated water with bands for ν_{as}, ν_{sym} in the 3500-3200 cm^{-1} range, and δ_{sym} at 1627cm^{-1}. All complexes also exhibit bands of H_2O ρ_r at 855, 848 and 843 cm^{-1}, and of ρ_w at 533, 527 and 527 cm^{-1}, respectively for **[CuPTPh]$^{2+}$**, **[CuPTB]$^{2+}$** and **[CuPTP]$^{2+}$** (Fig. S15), indicating the presence of coordinated water.

Electronic spectroscopy of the complexes in the UV-Vis region (Fig. S16) evidences intra-ligand π-π* transitions at 242 (ε = 20757 $M^{-1}\,cm^{-1}$), 261 (ε = 6083 $M^{-1}\,cm^{-1}$) and 260 (ε = 3428 $M^{-1}\,cm^{-1}$) nm, whereas d-d transitions were observed at 644 (ε = 174 $M^{-1}\,cm^{-1}$), 640 (ε = 96 $M^{-1}\,cm^{-1}$), and 640 (ε = 90 $M^{-1}\,cm^{-1}$), for **[CuPTPh]$^{2+}$**, **[CuPTB]$^{2+}$** and **[CuPTP]$^{2+}$**, respectively. The increased molar absorptivity of **[CuPTPh]$^{2+}$** is possibly due to electronic effects of the phenyl group in comparison to *n*-butyl or *n*-propanol substituents. A shoulder at 287 nm with molar absorptivity around 2000 $M^{-1}\,cm^{-1}$ was also observed in the electronic spectrum of **[CuPTB]$^{2+}$** and **[CuPTP]$^{2+}$**, possibly due to a ligand to metal charge-transfer transition.[25] Cyclic voltammetry of these complexes indicated a reversible redox Cu(II)-Cu(I) at 0.12, 0.14 and 0.16 V (*vs* Ag/AgCl/KCl 3.5 M) for complexes **[CuPTPh]$^{2+}$**, **[CuPTB]$^{2+}$** and **[CuPTP]$^{2+}$**, respectively (Fig. S21).

Nitrite Coordination

To obtain information whether nitrite coordinates to the copper complexes, the latter were treated with $NaNO_2$ in methanol, leading to immediate color change from blue to green, resulting from a shift of the d-d transition band at 644 nm to 580 nm in the case of complex **[CuPTPh]$^{2+}$** (Fig. 3A and S22). The nitrite complex also exhibits a band at 373 nm, which has been attributed to a metal-to-ligand charge transfer band.[15, 26]

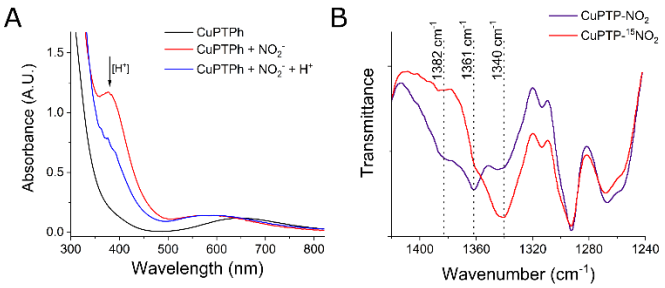

Fig. 3. UV-Vis Spectral changes of complex [**CuPTPh**]$^{2+}$ after addition of 1 eq. of $NaNO_2$ and addition of 1 eq. of benzoic acid (A) and FTIR spectra of complex [**CuPTP**]$^{2+}$ coordinated with NO_2^- and $^{15}NO_2^-$ using ATR-FTIR (B).

From FTIR experiments (Fig. 3B and S23) we can observe bands at 1377 cm^{-1} (**[CuPTPh(NO$_2$)]$^+$**), 1370 cm^{-1} (**[CuPTB(NO$_2$)]$^+$**) and 1361 cm^{-1} (**[CuPTP(NO$_2$)]$^+$**) that shift to lower wavenumbers upon the use of ^{15}N labelled nitrite. They can be associated to ν_{sym}(N-O) in κ^2O nitrito complexes [27]. However, since both κ^1N and κ^2O coordination modes exhibit bands in this region and that the ν_s(Cl-O) associated to the perchlorate anion could overlap with diagnostic bands such as ν_{sym}(N-O) arising from κ^2O ligation [28], the coordination mode of nitrite cannot be assigned unambiguously by FTIR. Therefore, an EPR spectroscopy study was performed to glean information about the environment around copper. The EPR spectra of Cu(II) complexes recorded in methanol at 296 K and 77 K are similar (Fig. S24), showing the four-line Hallmark pattern resulting from the hyperfine coupling of the electron spin of Cu(II) with the I = 3/2 nuclear spin of the $Cu^{63/65}$ isotopes (100% natural abundance). Additional super-hyperfine lines are observed after the addition of 1 equivalent of $NaNO_2$, which originates from coupling of the unpaired electron of Cu(II) with the bound nitrogen atoms. To verify if the super-hyperfine lines observed in the spectra can be attributed to a 3N or 4N coordinative environment, simulations were performed and compared with the first derivative of experimental EPR spectra (Fig. S25-27). The best fit should be the one that results in a line closer to a flat line or with minimal noise after the subtraction between simulation and experimental spectra. For instance, the spectrum of complex **[CuPTB]**$^{2+}$ without nitrite exhibits a greater similarity to the simulation with 3 N ligands (Fig. S25). After nitrite coordination, the simulated spectrum with 3 N ligands remains comparable to the experimental spectrum, indicating that the coordination of nitrite does not involve the nitrogen atom. Corroborating to this result is the EPR of **[CuPTP]**$^{2+}$ in the presence of $^{15}NO_2^-$, which presents similar first derivative spectra to the $^{14}NO_2^-$ coordination (Fig. S28). Considering these results, we propose that the complexes bear nitrite in a κ^2O coordination mode.

Since nitrite reduction necessitates protons (equation 1), we wanted to check the influence of an acidified medium. The addition of benzoic acid causes a decrease of the MLCT band at 373 nm that is characteristic of the Cu(II)-NO_2^- adduct (Fig. 3). The addition of a larger excess (100 eq.) results in an even higher decrease of the MLCT band (Fig. S31). To verify the possibility of forming a complex with nitrous acid (HONO), we performed ^{15}N-NMR spectroscopy on a mixture of **[CuPTP]**$^{2+}$ and ^{15}N-labeled nitrite, encouraged by previous work on ruthenium complexes[29] for which the coordination mode of nitrite could easily be verified by ^{15}N-NMR. However, the presence of Cu^{2+} in the NMR tube made the visualization of $^{15}NO_2^-$ impossible due to the paramagnetism of the metal ion. Therefore, a zinc version of the complex (**[ZnPTP]**$^{2+}$, Fig. S37-S39) was used to enable the ^{15}N-NMR analysis. The control without the complex and with $^{15}NO_2^-$ in the presence of 2 eq. of acetic acid did not show any $H^{15}NO_2$ (Fig. S32A), exhibiting only the signal that corresponds to nitrite at 611 ppm. The mixture between **[ZnPTP]**$^{2+}$ and nitrite resulted in a decreased visibility of the signal, however, a signal at 592 ppm is observed (Fig. S32A). Upon addition of 2 eq. of acetic acid, 3 signals were observed, which could arise from free[30] (599,08 ppm) and isomers of coordinated HNO_2 (598,86 and 598,43ppm, Fig. S32A). Since chemical shifts for O-coordinated nitrite are expected to be found around 580-600 ppm whereas the N-coordinated is observed at 460-480 ppm,[29] it is reasonable to affirm that for the **[ZnPTP]**$^{2+}$ complex, nitrite coordinates through oxygen, and that upon acidification, it forms a mixture between free and coordinated nitrous acid. In fact, **[ZnPTP(HNO$_2$)]$^+$** exhibits more intense vibrational modes of HONO in solution (Fig. S32B) upon acidification than **[CuPTP(HNO$_2$)]$^+$** (Fig. 3A), pointing to a possible equilibrium. Interestingly, after 24 hours, all the ^{15}N-NMR signals around 598 ppm in the acidified **[ZnPTP(NO$_2$)]$^+$** solution collapse into a single signal at 600 ppm (Fig. S32A), indicating that nitrous acid is released to the bulk solution over time while acetate binds to the complex. Similarly, after 24 hours, **[CuPTP(NO$_2$)]$^+$** that was in the presence of acid returns to its blue colour, with d-d transition centred at 610 nm (Fig. S33A), characteristic of the carboxylate complex (Fig. S48C). The formation of this complex was also evidenced by FTIR (Fig. S34) and HRMS with m/z found at 593.18512 (calculated for $C_{33}H_{32}CuN_5O_2$: 593.18465, Fig. S33B). DFT calculations also indicate an exergonic reaction for the generation of the nitrous acid complex with ΔG of – 153.2 , -159,0 and -154.1 kJ mol^{-1} for **[CuPTPh(NO$_2$)]$^+$, [CuPTB(NO$_2$)]$^+$** and **[CuPTP(NO$_2$)]$^+$,** respectively, pointing to a favourable proton transfer reaction (see SI).

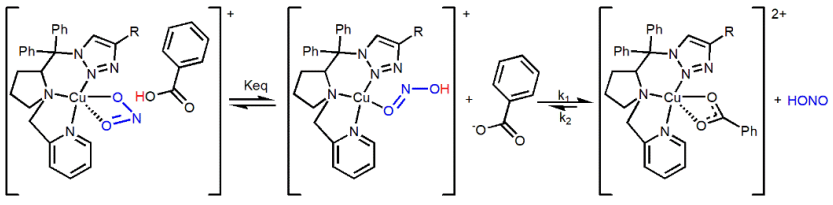

Scheme 2 Protonation of coordinated nitrite and the equilibrium between species in solution.

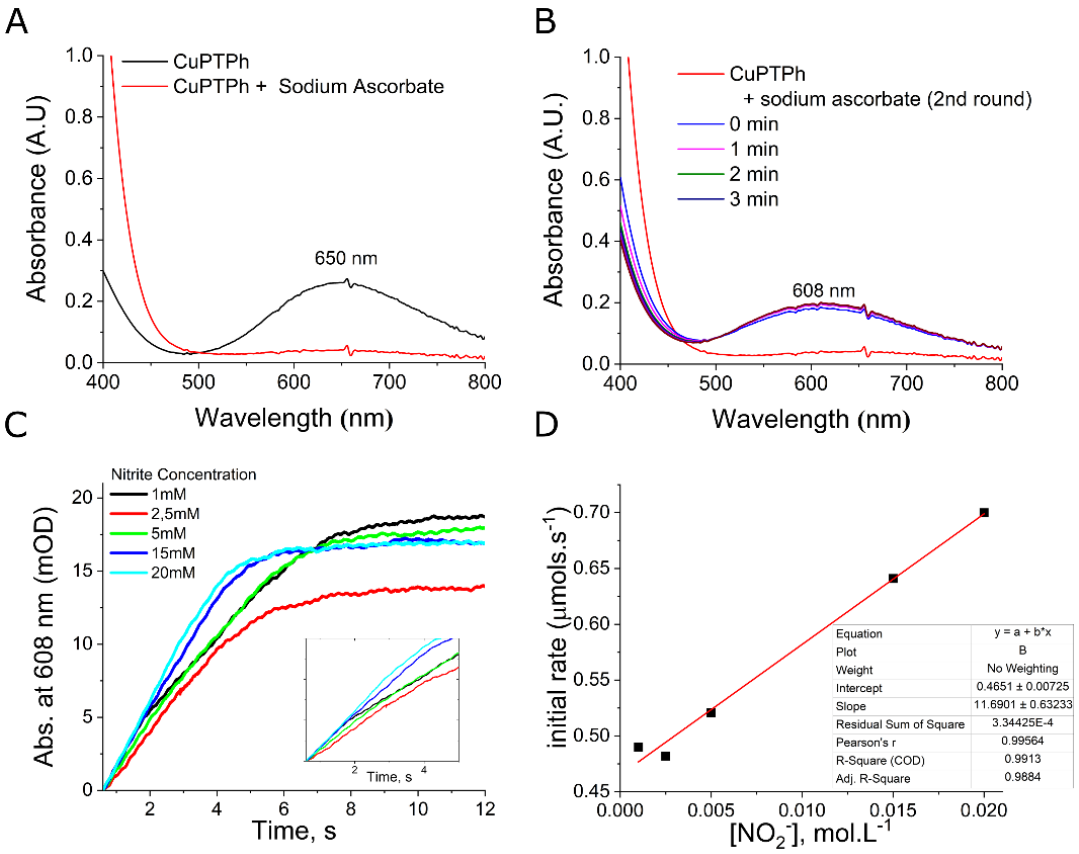

Fig. 4 Electronic spectrum of complex **[CuPTPh]²⁺** before (black line) and after (red line) addition of sodium ascorbate (A). After the addition of sodium nitrite, the d-d band of complex **[CuPTPh]²⁺** reappears. The appearance of the band at 608 was monitored over three minutes. After that, another round of sodium ascorbate addition was performed (red line), indicating the reversible nature of the reduction of the copper center (B). Stopped-flow measurement of complex **[CuPTP]²⁺** following the 608 nm band with time at different nitrite concentrations (C) and the decrease in initial rate of nitrite reduction by complex **[CuPTP]²⁺** upon nitrite concentration increase (D).

Moreover, the band at 373nm of the coordinated nitrous acid was also shown to have lower molar absorptivity than the band at 580nm band in DFT calculations (Fig.S60), corroborating to the experimental results.

Since this is an equilibrated reaction, it can be displaced back to bound HONO to **[CuPTP]²⁺** by the addition of 1 eq. of nitrite as evidenced by UV-Vis spectroscopy (Fig. S33A), but isolation of the **[CuPTP(HNO$_2$)]²⁺** complex failed due to its instability. [31, 32] In agreement with the NMR results is the EPR spectrum of the protonated nitrite complex, which does not superimpose with the one of the benzoate complex (Fig. S36). Nitrite coordination was also evidenced by cyclic voltammetry experiments. Addition of 50 equivalents of sodium nitrite to a 1 mM solution of the copper complexes in methanol shifts cathodically the Cu(II)/Cu(I) redox potential (Fig. S40-S42). In conclusion, UV-Vis, FTIR and EPR spectroscopies, and the shift in redox potential are all pointing to water displacement by nitrite in the coordination sphere of copper, in line with what is postulated for turning-over CuNiR enzymes. Therefore, we tested our copper complexes in catalytic NO_2^- reduction.

Nitrite Reduction

Nitrite reduction in CuNiRs is performed *via* the reduction of a Cu(II) center. To achieve this reduction, we used sodium ascorbate as a sacrificial electron donor. Ascorbate (Asc^-) has a $Asc^{\bullet}/Asc^-$ potential at 0.350 V (*vs* SHE),[33] which should be sufficient to reduce all three complexes. Addition of 1 equivalent of sodium ascorbate to a solution of the copper complexes in deaerated methanol under inert atmosphere immediately changed the color of the solution from blue to light yellow and the d-d transition band disappeared, indicating the reduction of the copper center (Fig. 4A). The Cu(I) state is stable for several minutes (> 40 min) under inert atmosphere and after the addition of 1 equivalent of sodium nitrite and 2 equivalents of benzoic acid, the d-d transition band rapidly reappears (Fig. 3B), indicating the re-oxidation of the copper center. In agreement with cyclic voltammetry, this process was shown to be reversible since the addition of subsequent aliquots of sodium ascorbate reduced the complex, and, after addition of nitrite, the copper was re-oxidized, as shown in Fig. 4B.

The rapid increase of the d-d transition band absorbance was monitored by stopped-flow UV-Vis measurements at a temperature of 10 °C (Fig. 4C). The reaction was followed at 608 nm by mixing fixed concentrations of the complexes, benzoic acid and ascorbate, with varied concentrations of NO_2^-. Upon increasing concentrations of substrate (final concentrations ranging from 1 mM – 20 mM), complexes **[CuPTB]²⁺** (Fig. S43C and D) and **[CuPTPh]²⁺** (Fig. S43 A and B) were inhibited, whereas complex **[CuPTP]²⁺** (Fig. S43C and D) was not. The lack of inhibition by nitrite in **[CuPTP]²⁺** indicated that most probably

a hydrogen transfer might be the limiting step. Evidence of the existence of a hydrogen bond between the propanol moiety and the labile ligand coordinated to the metal center can be seen in the comparison of the ^{1}H NMR spectra of the **[ZnPTP]$^{2+}$** complex and the free PTP ligand (Fig. S37): the OH signal from the *n*-propanol moiety is downfield shifted by almost 1 ppm, which is associated with a shortening of the H bond characteristic of hydrogen bonding[34] between *n*-propanol and coordinated water molecules. This phenomenon is likely to be reproduced for **[CuPTP]$^{2+}$**. Interestingly, photo-titration of **[CuPTP(NO$_2$)]$^+$** in the presence of the photoacid 2-NBA (2-nitro benzaldehyde) revealed a band that emerged at 978 cm^{-1} (Fig. S45) which was not found when **[CuPTP(NO$_2$)]$^+$** or 2-NBA were submitted to the same experiment. This suggests that this band may be the IR signature of the transferring proton in H-bonds.[35]

Moreover, as the product of 2-NBA photolysis is 2-nitro-benzoic acid, one can inspect the ratio between the carboxylic acid (1731 cm^{-1}) and the carboxylate (1650 cm^{-1}) ν(C=O) bands absorbances. This will give an estimate of the percentage of carboxylate present in solution, and thus whether a proton has been transferred to another species: the lower the ratio, the higher the number of proton transfer events. Indeed, the 10-fold ratio observed for 2-NBA was lowered to 4.5 in the presence of **[CuPTPh(NO$_2$)]$^+$** and is even lower in the presence of **[CuPTP(NO$_2$)]$^+$** (1.7), corroborating with the ability of *n*-propanol to assist proton transfer (Fig. S46). Interestingly, DFT calculations revealed that upon addition of a water molecule in the open coordination site of the complex, the highest gain in energy is observed for [**CuPTP(NO$_2$)H$_2$O**]$^+$ (ΔG = -18.1 kJ mol^{-1}), revealing that the propanol moiety is stabilizing the nitrous acid in a higher extent than the other pending groups ([**CuPTPh(NO$_2$)H$_2$O**]$^+$ with ΔG = -10.3 kJ mol^{-1} and [**CuPTB(NO$_2$)H$_2$O**]$^+$ with ΔG = -10.1 kJ mol^{-1}), in agreement with our experimental data.

Catalytic assays were performed using 10 mol% of the copper complexes in methanol using 2 equivalents of benzoic acid. The reaction was initiated by the addition of sodium ascorbate. A N_2 flow removed the gaseous content from the reaction flask to a second reaction flask containing citrate buffer (0.1 M, pH=5) and [Fe(EDTA)]$^{2-}$ to enable the detection of NO.[36] After 10 minutes of reaction, the flask containing [Fe(EDTA)]$^{2-}$ exhibited a yellow colour and the characteristic band at 432 nm for [Fe(EDTA)(NO)] (Fig. S44). The values of detected NO as [Fe(EDTA)(NO)] were compared to a control reaction using sodium nitrite in acidic medium. Using these conditions, the percentage of detected NO was 73.5% (±1.2), 61.7% (±4.0) and 96.8% (±0.9) for complexes **[CuPTPh]$^{2+}$**, **[CuPTB]$^{2+}$** and **[CuPTP]$^{2+}$**, respectively. Under the same conditions [ZnPTP]$^{2+}$ generated only 1.3% of NO, whereas without the copper complexes, the band at 432 nm was not observed, indicating the catalytic nature of the complexes and superior kinetics with respect to nitrous acid disproportionation.

Monitoring of the UV-Vis spectral changes of a stepwise addition of nitrite to **[CuPTP]$^{2+}$**, followed by its reduction by sodium ascorbate and the addition of acetic acid, reveals that upon reduction of **[CuPTP(NO$_2$)]$^+$**, nitrite remains bound to the complex, as the ligand to metal charge transfer band at 373 nm is left unchanged, whereas the d-d band fades away with a k_{obs} of 9 s^{-1} (Fig. S47A). Addition of acetic acid to the reduced **[CuPTP(NO$_2$)]$^+$** reveals the decrease in the ligand-to-metal charge transfer band (k_{obs} of 15 s^{-1}) and a concomitant increase of the d-d band (Fig. S47B), which shifts from the initial 658 nm to 610 nm, as expected for an acetate complex. Interestingly though, when copper is reduced, no vibrational features of HONO are observed when acid is added, indicating that k_{cat} is faster than k_1 (Scheme 2). Therefore, a proposed mechanism for the catalytic reduction of nitrite by the copper complexes follows the displacement of water molecules from the coordination sphere, resulting in a κ^2O coordination mode. Upon acidification, there is a change of coordination mode to κ^1O (Cu–ONOH), which is rapidly followed by the electron reduction of the copper complex. Then, the next step involves another protonation of nitrite and an electron transfer from Cu(I) to nitrite, which could go through different mechanisms (PCET, PT-ET, ET-PT, etc [37]). To differentiate between these mechanisms, the KIE (kinetic isotope effect) of the reaction was determined by the ratio between k in methanol-H_4 and methanol-D_4 (Fig. S48). A KIE of 0.3 was obtained, which can be explained by an equilibrium isotope effect on the initial proton transfer, consistent with a PT-ET [37] mechanism for NO evolution and in agreement with other studies reporting inverted KIE.[38, 39] In this step, benzoate coordinates to the copper complexes, aiding the evolution process, as shown in Fig. 5. As evidenced by UV-Vis spectroscopy, benzoate can be displaced by excess nitrite (Fig. S33A), recycling the catalyst. The competition between benzoate and nitrite and the displacement of benzoate is also in agreement to the slightly higher binding constant of nitrite (2.6×10^3 M^{-1}) in comparison to benzoate (1.8×10^3 M^{-1}), which were determined with the Benesi-

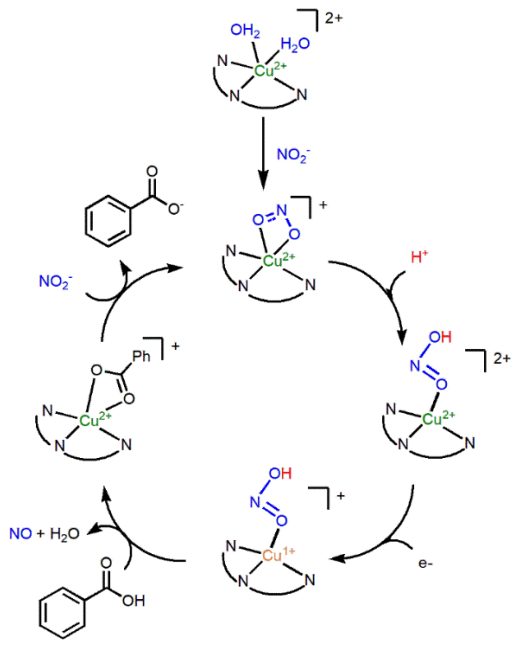

Fig. 5 Mechanistic proposal for the nitrite reduction with the copper complexes reported in this article. A change in the coordination mode of the nitrite anion is observed upon protonation, which was shown to be regulated by the ligand.

Hildebrand method (Fig. S49), similarly to Carmona-Vargas *et al*.[40]

Electrocatalytic Nitrite Reduction

Noticing that the copper complexes were able to reduce nitrite in the presence of acid and a reducing agent to evolve NO, we decided to evaluate the electrocatalytic ability of these systems. Analogous to the chemical redox mechanism, nitrite is still coordinated to the copper complex after applying potential, as evidenced by the spectro-electrochemical assay (Fig. S50), which indicates a shift of the LMCT from 373 nm to 360 nm whereas the d-d band decreases with the increase of applied potential. Interestingly, after the addition of benzoic acid, an increase in the reduction current was observed, indicative of catalysis. The higher the acid concentration, the higher the reduction current of the Cu(II)/Cu(I) couple (Fig. 6). All complexes presented a catalytic current at a 50 mV s^{-1} scan rate. The spectro-electrochemistry of a 0.5 mM methanolic solution of **[CuPTP(NO$_2$)]$^+$** in the presence of 1 mM benzoic acid and 0.5 mM $NaNO_2$ under a potential of –0.24 V evidenced the decrease of the ligand to metal charge transfer and the d-d bands (Fig. S51). Complex **[CuPTPh]$^{2+}$** presented a higher current with the increase of benzoic acid concentration, as shown in Fig. 6, indicating a faster reaction of the reduced Cu(I) complex with nitrite, which is followed by complexes **[CuPTP]$^{2+}$** and **[CuPTB]$^{2+}$**. This trend follows the $E_{½}$ of the complexes with nitrite (Fig. S40-S42), in which complex **[CuPTPh]$^{2+}$** exhibits the lowest value. Bulk electrolysis was performed with the application of fixed potential at –0.1 V for 2 h and NO was detected by complexation with CoTPP[27] solubilized in dichloromethane, that was inserted into an open flask in the electrochemical cell but separated from the electrochemical solution. At the end of the experiment, an aliquot of this solution was also taken, and a UV-Vis spectrum was recorded. The shift of the Soret and the Q bands were in agreement with NO coordination(Fig. S52) [41] and was not observed without the complexes (Fig. S52). Noticing that the λ_{max} of CoTPP shifts with increasing level of complexation to NO and that λ_{max} at 538nm indicates a 100% NO complexation[20], we assume a Faradaic yield of 99%. The infrared spectrum also confirms the coordination of NO with the appearance of an intense band at 1695 cm^{-1} that is characteristic of ν(N-O) [41] (Fig. S53). At the end of the catalytic experiment, the recorded cyclic voltammogram was typically unchanged from the ones of the catalysts alone (Fig. S40-S42). Interestingly though, isolated benzoate complex has a reduction process centered at –0.08 V and the isolated nitrite complex in the presence of benzoic acid shifts the reduction from 0.02 V to –0.02 V, indicating that the benzoate complex is formed in the reaction. However, addition of perchloric acid shifts the redox process to +0.08 V, suggesting the restoration of the starting aquo complex (Fig. S54). Therefore, the mechanism of electrocatalysis should be analogous to the one proposed for the chemical reduction with ascorbate (Fig. 5).

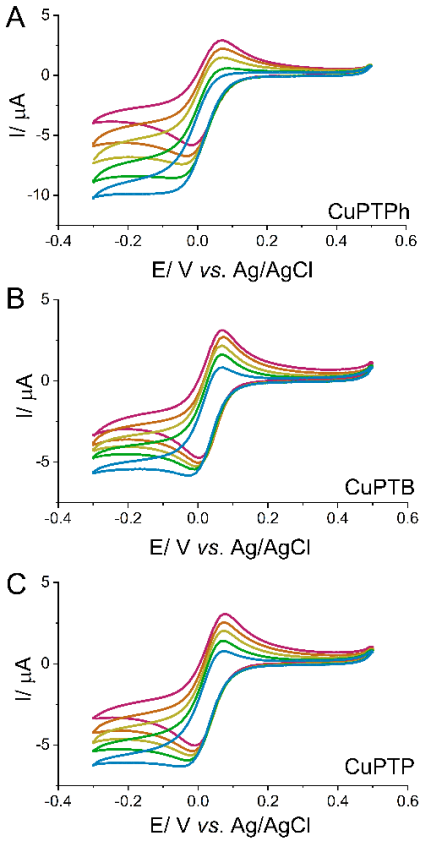

Fig. 6 Cyclic voltammogram of the copper complexes in the presence of 50 eq. of $NaNO_2$ and increasing amounts of benzoic acid: 0 eq. (black line), 2 eq. (red line), 5 eq. (blue line), 10 eq. (pink line) and 22 eq. (green line). The experiments were performed in methanol, using 0.1M TBAP as electrolyte and scanning rate of 50 mV/.

The kinetics of nitrite reduction were also evaluated by cyclic voltammetry, by changing the amount of nitrite present in the electroreduction catalysis (Fig. 7A, S55 and S56). The current intensity can be converted to obtain the production of nitric oxide (V_{NO}) per unit of electrode area.[20] These data enabled the construction of a graphic of V_{NO} *versus* nitrite concentration as a Michaelis-Menten kinetic curve (Fig. 7B), following equation (2).

$$V_{[NO]} = V_{max}[NO_2^-] / (K_M + [NO_2^-]) \qquad (2)$$

The obtained values of V_{max} and K_M for all complexes are shown in Table 1. The V_{max} values can be converted to k_{cat} by dividing it by the complex concentration. As the concentration of the

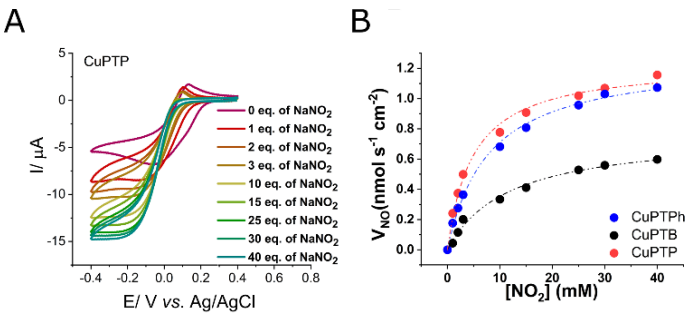

Fig. 7 Cyclic voltammogram of complex [CuPTP]$^{2+}$ in the presence of 100 eq. benzoic acid and increasing amounts of sodium nitrite (A) and the Michaelis-Menten curve for the copper complexes obtained from these experiments (B). The experiments were performed in methanol, using 0.1 M PTBA as electrolyte and scan rate of 50 mV s^{-1}.

complex active in the reaction is related to the electrode surface in the cyclic voltammetry experiment, the concentration can be determined by the integral of the charge in the reversible redox process in the absence of substrate (value of 2.5×10^{-10} mol cm^{-2}). Interestingly, the catalytic efficiency (k_{cat}/K_M) of complex **[CuPTP]$^{2+}$** is similar to the one reported for a tetradentate copper complex based on tris(2-methylpyridyl)amine (1200 M^{-1} s^{-1}).[20] This indicates that the propanol moiety of complex **[CuPTP]$^{2+}$** may assist the proton transfer to nitrite, corroborating to our results from stopped-flow analysis.

Table 1 Thermodynamic and kinetic data for the three complexes determined by electrochemistry.

	[CuPTPh]$^{2+}$	[CuPTB]$^{2+}$	[CuPTP]$^{2+}$
E½ (V)	0.02	0.06	0.03
V_{max} (nmol s^{-1}cm^{-2})	1.27	0.76	1.24
K_M (mM)	7.86	11.7	4.87
k_{cat} (s^{-1})	5.08	3.04	4.92
k_{cat}/K_M (M^{-1} s^{-1})	646.3	259.8	1010.2

Discussion

Nitrite coordination and protonation

Coordination of nitrite to the copper complexes was assessed by UV-Vis, FTIR, EPR, CV, microanalysis, and conductivity, pointing to a κ^2O coordination mode for the oxyanion. In the literature, complexes bearing this coordination mode typically bear the hydrotris(pyrazolyl)borate or bis[2-(1-methylbenzimidazole-2-yl)methyl]amine ligands, in which the bulkiness of the substituents interfere in the symmetry of coordination[42]. In CuNiR enzymes, nitrite binds asymmetrically[43]. However, as the symmetric and asymmetric nitrite κ^2O coordination does not reveal any significant differences in the UV-Vis and FTIR spectroscopies[43], and as our attempts to crystallize the nitrito complex failed, we can't ascribe if nitrite is coordinated symmetrically or asymmetrically. EPR spectroscopy of **[CuPTB]$^{2+}$** evidences an anisotropy that corroborates to the distorted square pyramidal structure observed by sc-XRD (g[x y z] of 2.042, 2.078 and 2.250, table S2). Interestingly though, a more axial complex is formed upon nitrite coordination to form **[CuPTB(NO$_2$)]$^+$** (g_x and g_y of 2.055 and 2.052 and g_z= 2.234), indicative of a dz^2 ground state[28] and axial EPR spectroscopy has been correlated to an asymmetric nitrite coordination to copper complexes [28, 43].

Acidification of the nitrito complexes resulted in a decrease of the MLCT band at 373 nm (Fig. 2), indicating that either nitrite is dissociating or that the nitrite is changing its coordination mode. It is possible to notice five-finger like bands under the MLCT band in the UV-Vis of acidified **[CuPTPh(NO$_2$)]$^+$**. This is indicative of the formation of free HONO. However, this reaction is governed by three different dissociation constants: the pK_as of nitrous and benzoic acid and the dissociation constant of the nitrous acid complex. Thus, most probably there is an equilibrium reaction that passes from **[CuPTPh(NO$_2$)]$^+$** to **[CuPTPh(HNO$_2$)]$^{2+}$** to generate **[CuPTPh(benzoate)]$^+$** and free HONO. Interestingly, the EPR spectra of **[CuPTPh(NO$_2$)]$^+$** before and after acidification are different than the EPR of isolated **[CuPTPh(benzoate)]$^+$**. This points to a metastability of complex **[CuPTPh(HNO$_2$)]$^{2+}$**, which was also observed in the ^{15}N NMR of (**[ZnPTP(^{15}NO$_2$)]$^+$**). As we were able to observe the meta-stable intermediates of **[ZnPTP(^{15}HNO$_2$)]$^{2+}$** via ^{15}N NMR even though the five-finger bands from free HONO are stronger in its UV-Vis than **[CuPTP(HNO$_2$)]$^{2+}$**, it is possible to infer that **[CuPTP(HNO$_2$)]$^{2+}$** is also formed upon acidification of **[CuPTP(NO$_2$)]$^+$**. However, it should be noted that generation of free HONO only occurs under non-catalytic conditions, as the five-finger bands of HONO are not observed for the reduced copper complex (Fig. S47). Moreover, upon reduction of the copper centre to Cu^{1+}, nitrite could exhibit two different coordination modes: κ^1N[27], common for Cu^{1+} complexes [24, 44], and κ^2O. Our experimental evidence does not suggest a coordination mode change upon copper reduction. For instance, the reverse KIE observed in our systems indicate that protonation is a necessary pre-equilibrium prior to the rate-determining step. This means that any reorganization in coordination mode most probably occur at the protonation step, as the isomerization of nitrite is a slow process[27].

Nitrite reduction comparison to other copper complexes

The presence of ascorbate, benzoic acid, and copper complexes (**[CuPTPh]$^{2+}$**, **[CuPTB]$^{2+}$**, and **[CuPTP]$^{2+}$**) during the catalytic reduction of nitrite resulted in significant yields of NO production. An interesting study by Woolard-Shore *et al.* [45] reported on the reduction of nitrite using copper complexes

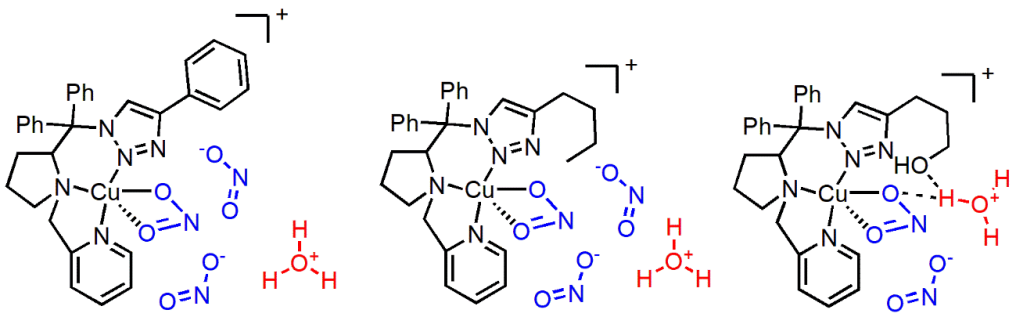

Fig. 8 Schematic view of the proposed interaction between the copper complexes with nitrite and hydronium. The phenyl group from complex **[CuPTPh(NO$_2$)]$^+$** enables a more exposed active site and nitrite electrostatically interact with the complex (A). Complex **[CuPTB(NO$_2$)]$^+$** has a bulky n-butane that might repel some of the nitrite, but still allows nitrite to electrostatically interact with the complex (B). Complex **[CuPTP(NO$_2$)]$^+$** can hydrogen-bond to hydronium, assisting proton transfer to the active site (C).

coordinated to trien-based ligands. Surprisingly, despite employing similar reducing conditions with *L*-ascorbic acid in a methanolic solution, they observed preferential N_2O production by some of the complexes, even though NO was also generated in yields ranging from 25% to 100%[45]. The differences in product formation could not be attributed solely to the redox potentials of the complexes. Thus, Timmons and Symes[46] attempted to explain these variations based on the N-O bond length of the complexes. Interestingly though, complexes with lower steric hindrance were found to generate N_2O. Notably, nitrous oxide can be formed as a result of nitric oxide coupling, leading to the formation of dimeric species[22]. This suggests that dimerization may play a significant role in N_2O production. Given the high yields of NO observed in our complexes, we hypothesize that our complexes are less prone to dimerization compared to those reported by Woolard-Shore *et al.*[45].

Comparison to the biological system

The three complexes evaluated in this work were designed to bear a N,N,N coordination motif with slight differences in the secondary coordination sphere to evaluate their ability in mimicking CuNiR activity. Interestingly, sc-XRD revealed the presence of two water molecules coordinated to the copper center, achieving a square pyramidal geometry. This geometry found in the first coordination sphere recalls a similar, recent observation of two water molecules coordinated to the copper center of a CuNiR enzyme. Rose *et al.*[18] described that one water molecule is more strongly coordinated to the copper centre than the other one, with Cu–O bond lengths of 1.940 and 2.162 Å. In comparison, complex **[CuPTPh]$^{2+}$** exhibits Cu–OH_2 bond lengths of 2.010(4) (Cu–O2) and 2.354(4) Å (Cu–O1), the apical water molecule being the remote one. The longest Cu–N bond is Cu-N4 (2.073(3) Å), probably due to the steric hindrance caused by the substituents of the sp^3-hybridized nitrogen. The lengths of the Cu-N2 and Cu-N5 bonds are similar and shorter, measuring 1.954(4) and 1.951(4) Å, respectively. These distances are comparable to the Cu-$N_{(His)}$ distances found at the T2Cu site in the CuNiRs of *Br*^{2D}NiR. Therefore, we would expect to observe catalytic similarities between the complexes and CuNiRs of *Br*^{2D}NiR.

The catalytic efficiency (k_{cat}/K_M) of complex **[CuPTP]$^{2+}$** is 1010 M^{-1} s^{-1}, whereas **[CuPTPh]$^{2+}$** and **[CuPTB]$^{2+}$** present values of 646 and 259 M^{-1} s^{-1}, respectively. The k_{cat}/K_M of CuNiR enzymes with just one water molecule coordinated to the active site, such as AxNiR,[47] is of the order of 10^6 M^{-1} s^{-1} [48, 49]. However, two-water coordinated CuNiR, such as *Br*^{2D}NiR, present a decreased catalytic efficiency of ~100 fold in comparison, and k_{cat}/K_M is expected to be around 10^4 M^{-1} s^{-1}. This catalytic efficiency is only one order of magnitude higher than the one obtained for complex **[CuPTP]$^{2+}$**, indicating a good resemblance of complex **[CuPTP]$^{2+}$** with the active site of *Br^{2D}NiR*. Moreover, complex **[CuPTP]$^{2+}$** was the most efficient catalyst both in electrocatalysis and chemical reduction. This complex has a pendent propanol group that could serve as a gatekeeper for protons and as a proximal ligand in a way that mimics aspartate residue of the active site of CuNiR. Nitrite reduction to NO upon copper(I) protonation has been described, [19, 50-52] leading to the formulation of a proton-coupled electron transfer pathway. [9, 20] Therefore, hydrogen bond-making secondary sphere ligands are supposed to increase the activity of nitrite reduction. For instance, in CuNiR, protons are the substrate and gate the electron transfer from T1Cu to T2Cu.[18] Nitrite initially binds side-on by the displacement of the water ligands, followed by the protonation of histidine and the formation of a CuNOOH intermediate. This triggers a proton-coupled electron transfer that leads to the reduction of nitrite via HO–NO bond breakage to nitric oxide and water, leaving NO coordinated to the copper center in a side-on manner. There is only one report with spectroscopic evidence of the formation of a biomimetic copper-nitrosyl species prior to NO evolution, under nitrite reduction conditions.[27] Alternatively, an inorganic model was described to bypass the nitrosyl complex formation via the involvement of the secondary coordination sphere in H^+/e^- transfer events. [6] Outer coordination sphere was also shown to be important in phenol-mediated reduction of nitrite to NO via proton-coupled electron transfer. [6, 9] These literature data all point to the fact that the second coordination sphere plays an important role in the reduction pathway. Comparatively, our work strongly suggests that the pendent propanol aids the protonation step by possibly stabilizing the Cu-ONOH intermediate, which results in complex **[CuPTP]$^{2+}$** being a more efficient catalyst than the two other complexes (Fig. 8). When considering complexes **[CuPTB]$^{2+}$** and **[CuPTP]$^{2+}$**, the substitution of a methyl group to an alcohol moiety increases the catalytic efficiency by a factor of almost 4-fold.

Moreover, stopped flow measurements indicated that nitrite reduction to NO was inhibited at high substrate concentrations when using **[CuPTB]$^{2+}$** (Fig. S43C and D) and **[CuPTPh]$^{2+}$** (Fig. S43 A and B) as complexes. On the other hand, **[CuPTP]$^{2+}$** was not inhibited. Interestingly, *Rp*NiR-core protein have been shown to be inhibited by high nitrite concentrations,[53] as well as *Ax*NiR variants in which the residues involved in proton channeling were mutated. [54] The inhibition was tentatively explained by the binding of a second nitrite molecule or by the occurrence of different reduction pathways in the reaction cycle with slower rates becoming dominant at higher substrate concentration.[54] The slower route was ascribed to electron transfer (ET) as a rate-limiting step, but since it was previously shown that the ET is kinetically coupled to proton transfer[55], the proton transfer was more likely to be the rate-limiting step of the *Ax*NiR variants.[54] Thus, we suspect that the *n*-propanol moiety in complex **[CuPTP]$^{2+}$** may play the role of "proton channel" and therefore facilitate the proton transfer, whereas the phenyl (**[CuPTPh]$^{2+}$**) or *n*-butyl (**[CuPTB]$^{2+}$**) group are not likely to assist this step. For example, considering that the copper complexes are positively charged even after nitrite coordination (Scheme 2), it is evident that there is a higher attraction for the negatively charged nitrite than for the hydronium cation (Fig. 4). Thus, an increase in nitrite concentration can block the entrance of H_3O^+ into the catalytic site, inhibiting catalysis. The bulkiness and greater mobility of *n*-butyl in comparison to phenyl may block the interaction between the complex and additional nitrite molecules having a higher impact on the proton transfer step and result in a more pronounced inhibition by nitrite for complex **[CuPTB]$^{2+}$** (Fig. 4B). On the other hand, the *n*-propanol moiety can aid the delivery of hydronium in proximity of the active site by the formation of hydrogen bonds, as shown in Fig.

4C. ^{1}H NMR of **[ZnPTP]$^{2+}$** revealed the presence of hydrogen bonds between n-propanol moiety and bound water, which is likely reproduced in **[CuPTP]$^{2+}$** system. Phototitration experiments monitored by FTIR also evidenced that **[CuPTP]$^{2+}$** presented a higher degree of hydrogen transfer from a photogenerated acid than the other complexes, which was also shown in DFT calculations. This property is linked to the increased nitrite reduction activity of **[CuPTP]$^{2+}$** both chemically and electrochemically. Moreover, the reverse KIE reveals that the proton transfer occurs prior to the electron transfer. Hence, the stability of **[CuL(HNO$_2$)]$^{2+}$** is important to favour the reaction and most probably the hydrogen bond formed in **[CuPTP(HNO$_2$)]$^{2+}$** stabilizes it over **[CuPTPh(HNO$_2$)]$^{2+}$** and **[CuPTB(HNO$_2$)]$^{2+}$**. These results indicate a certain similarity between **[CuPTP]$^{2+}$** system and the biological catalyst and could be used to explore open questions regarding CuNiR activity and mechanism.

Conclusions

We have synthesized three different copper complexes that are able to reduce nitrite into nitric oxide. The reduction was performed either using sodium ascorbate or via electrocatalysis. In both methodologies, the most efficient catalyst carried a pendent *n*-propanol moiety in the secondary coordination sphere, pointing to a proton transfer assistance by the hydroxyl group. Interestingly, upon increasing amounts of substrate, the reaction seemed to be inhibited in the complexes where the *n*-propanol substituent was replaced with a *n*-butyl or phenyl group. Catalysis inhibition by increasing nitrite concentrations was only demonstrated in the enzyme, and this is the first example of a biomimetic complex that exhibits similar behavior, as demonstrated by stopped-flow analysis. It would be interesting to verify if closer proximity of the pendant hydrogen-bond acceptor near the copper center could improve catalytic efficiency to a value approaching the one of the enzymes.

Experimental Methods

Synthesis of the complexes CuPTPh, CuPTB and CuPTP

Synthesis of CuPTPh

To 6 mL of methanol were added 55 mg of Cu(ClO_4)$_2$.6H$_2$O (0.148 mmol) and 70 mg (0.148 mmol) of ligand PTPh. The reaction proceeded at 50 °C for 4 hours. After that, the solvent was removed under reduced pressure. To remove any free ligand the blue solid was washed with diethyl ether and dried, resulting in 102 mg (90% yield). Conductivity (μS cm^{-1}): 140.7 ± 0.7. HRMS (m/z): isotopic cluster found 534.1719 (CuPTPh$^+$) (calc 534.1718). FTIR in KBr (cm^{-1}) : 3386, 3447, 3521; 1637, 1612; 1481, 1448; 1148,1117, 1086; 765, 711. Anal. Calcd for $C_{31}H_{33}Cl_2CuN_5O_{10}$: C 48.35; H 4.32; N 8.25. Found: C: 47.95; H: 4.24; N 8.69.

Synthesis of CuPTB

To 6 mL of methanol were added 65 mg of Cu(ClO_4)$_2$.6H$_2$O (0.177 mmol) and 80 mg (0.177 mmol) of ligand PTB. The reaction proceeded at 50 °C for 4 hours. After that, the solvent was removed under reduced pressure. To remove any free ligand the blue solid was washed with diethyl ether and dried, resulting in 117 mg (90% yield). Conductivity (μS cm^{-1}): 146.7 ± 0.2. HRMS (m/z): isotopic cluster found 613.1519 (CuPTB$^+$) (calcd 613.1517). FTIR in KBr (cm^{-1}) : 3556, 3484, 3442; 1646, 1624; 1501, 1457; 1153 ,1127, 1097; 772, 719. Anal. Calcd for $C_{29}H_{37}Cl_2CuN_5O_{10}$: C 46.44; H 4.97; N 8.47. Found: C: 46.09; H: 4.82; N 8.63.

Synthesis of CuPTP

To 6 mL of methanol were added 58 mg of Cu(ClO_4)$_2$.6H$_2$O (0.158 mmol) and 72 mg (0.158 mmol) of ligand PTP. The reaction proceeded at 50 °C for 4 hours. After that, the solvent was removed under reduced pressure. To remove any free ligand the blue solid was washed with diethylether and dried, resulting in 108 mg (90% yield). Conductivity (μS cm^{-1}): 152.3 ± 0.1. HRMS (m/z): isotopic cluster found 516.1824 (CuPTP$^+$) (calcd 516.1824). FTIR in KBr (cm^{-1}) : 3551, 3471, 3417; 1638, 1616; 1493, 1449; 1146 ,1119, 1087; 766, 711. Anal. Calcd for $C_{29}H_{37}Cl_2CuN_5O_{11}$: C 45.53; H 4.74; N 9.15. Found: C: 45.26; H: 4.37; N 8.64.

Synthesis of [CuPTPhNO$_2$)]ClO$_4$

To 100 mL of a 0.1M CuPTPh (8mg) methanolic solution was added 50 mL of 0.2M $NaNO_2$ methanolic solution. The green solution was evaporated and washed 3 times with 100 mL of water. Then, the solid was resolubilized in methanol, dried with $MgSO_4$, filtered and evaporated, resulting in a green solid (5mg, 73% yield). Conductivity (μS cm^{-1}): 51.0 ± 0.1. HRMS (m/z): isotopic cluster found 534.1719 (CuPTPh$^+$) (calc 534.1718). FTIR in KBr (cm^{-1}): 1377. Anal. Calcd for $C_{31}H_{29}ClCuN_6O_6$: C 54.71; H 4.29; N 12.35. Found: C: 54.43; H: 4.25; N 12.47.

Synthesis of [CuPTB(NO$_2$)]ClO$_4$

To 10 mL of a 0.1M CuPTB (8mg) methanolic solution was added 5 mL of 0.2M $NaNO_2$ methanolic solution. The green solution was evaporated and washed 3 times with 10 mL of water. Then, the solid was resolubilized in methanol, dried with $MgSO_4$, filtered and evaporated, resulting in a green solid (7mg, 78% yield). Conductivity (μS cm^{-1}): 54.0 ± 0.1. HRMS (m/z): isotopic cluster found 613.1519 (CuPTB$^+$) (calcd 613.1517). FTIR in KBr (cm^{-1}): 1370. $C_{28}H_{35}CuClN_6O_6$: C 49.27; H 5.17; N 12.31. Found: C: 48.91; H: 4.93; N 11.99.

Synthesis of [CuPTP(NO$_2$)]ClO$_4$

To 10 mL of a 0.1M CuPTB (8mg) methanolic solution was added 5 mL of 0.2M $NaNO_2$ methanolic solution. The green solution was evaporated and washed 3 times with 10 mL of water. Then, the solid was resolubilized in methanol, dried with $MgSO_4$, filtered and evaporated, resulting in a green solid (8mg, 88% yield). Conductivity (μS cm^{-1}): 55.0 ± 0.1. HRMS (m/z):): isotopic cluster found 516.1824 (CuPTP$^+$) (calcd 516.1824). FTIR in KBr (cm^{-1}): 1382, 1361. Anal. Calcd for $C_{27}H_{33}ClCuN_6O_9$: C 47.37; H 4.86; N 12.28. Found: C: 47.61; H: 4.52; N 12.32.

Synthesis of CuPTPh-Benzoate

To 63 mL of a 0.1M CuPTPh (5mg) methanolic solution was added 50 mL of 0.2M sodium benzoate methanolic solution. The

blue solution was evaporated and washed 3 times with 100 mL of water. Then, the solid was resolubilized in methanol, dried with $MgSO_4$, filtered and evaporated, resulting in a blue solid (4mg, 81% yield). Anal. Calcd for $C_{38}H_{34}ClCuN_5O_6$: C 60.39; H 4.53; N 9.27. Found: C: 60.61; H: 4.52; N 8.98.

Author Contributions

Conceptualization M.P.F., A.S. and G.C.M.N.; Validation M.P.F., C.B.C., C.E., W.G.G.J., A.F.M., O.R.N., A.S., C.G.C.M.N.;Formal Analysis M.P.F., C.B.C., J.H., S.H. C.E., W.G.G.J., A.F.M E.E.C., D.R.T., O.R.N., A.S. and C.G.C.M.N.; Writing M.P.F, A.S. D.R.T., A.S and C.G.C.M.N.; Supervision C.G.C.M.N.

Conflicts of interest

There are no conflicts to declare.

Acknowledgements

We kindly acknowledge CAPES (88882.332767/2019-01) for the Ph.D. fellowship. DRT would like to thank FAPESP Grant 2019/17483-0 and 2013/07937-8. O.R.N. thanks CNPq (project 302186/2019-0). J.H and E.E.C would like to thank FAPESP grant 2021/04876-4. S. He acknowledges the financial support from the National Science Foundation (CHE-2004080). We would also like to thank CAPES project 001. We thank prof. R. Brian Dyer for the given research and financial support. This research had no other funding, despite the requirement of the financial support agencies for productivity.

References

1. M. Kern and J. Simon, in *Methods in Enzymology*, Elsevier, 2011, vol. 486, pp. 429-446.
2. E. v. Faassen, A. F. Vanin and A. Slama-Schwok, *Nitrite as Endothelial NO Donor under Anoxia*, Elsevier B.V, 2007.
3. A. B. Knott and E. Bossy-Wetzel, *Antioxidants Redox Signal*, 2009, **11**, 541–553.
4. D. Hao, Y. Liu, S. Gao, H. Arandiyan, X. Bai, Q. Kong, W. Wei, P. K. Shen and B. J. Ni, *Mater Today*, 2021, **46**, 212-233.
5. T. Liu, G. Li, X. Wu, S. Chen, S. Zhang, H. Han, H. Zhang, X. Luo, X. Cai and D. Ma, *Drug Deliv*, 2021, **28**, 306-318.
6. C. M. Moore and N. K. Szymczak, *Chem Sci*, 2015, **6**, 3373-3377.
7. S. Hematian, M. A. Siegler and K. D. Karlin, *J. Biol. Inorg. Chem*, 2014, **19**, 515–528.
8. W. J. Chuang, M. Narwane, H. Y. Chen, C. L. Kao, B. Huang, K. M. Hsu, Y. M. Wang and S. C. N. Hsu, *Dalton Trans*, 2018, **47**, 13151–13157.
9. A. Mondal, K. P. Reddy, J. A. Bertke, S. Kundu and S. Kundu, *J Am Chem Soc*, 2020, **142**, 1726–1730.
10. Y. Zhou, F. Bihl, A. Bonnefont, C. Boudon, L. Ruhlmann and V. Badets, *J Catal*, 2022, **405**, 212-223.
11. N. Castiglione, S. Rinaldo, G. Giardina, V. Stelitano and F. Cutruzzolà, *Antioxidants & Redox Signaling* 2012, **17**, 684-716.
12. Y. Li, M. Hodak and J. Bernholc, *Biochem*, 2015, **54**, 1233-1242.
13. R. W. Strange, L. M. Murphy, F. E. Dodd, Z. H. L. Abraham, R. R. Eady, B. E. Smith and S. S. Hasnain, *J Mol Biol*, 1999, **287**, 1001-1009.
14. Y. Fukuda, K. K. Yu Hirano, T. Inoue and T. Tamada, *Proc Nat Acad Sci*, 2020, **117**, 4071-4077.
15. F. Roncaroli, M. E. Ruggiero, D. W. Franco, G. L. Estiú and J. A. Olabe, *Inorg Chem*, 2002, **41**, 5760–5769.
16. K. Kataoka, H. Furusawa, K. Takagi, K. Yamaguchi and S. Suzuki, *J Biochem*, 2000, **127**, 345–350.
17. Y. Zhao, D. A. Lukoyanov, Y. V. Toropov, K. Wu, J. P. Shapleigh and C. P. Scholes, *Biochem*, 2002, **41**, 7464–7474.
18. S. L. Rose, S. V. Antonyuk, D. Sasaki, K. Yamashita, K. Hirata, G. Ueno, H. Ago, R. R. Eady, T. Tosha, M. Yamamoto and S. S. Hasnain, *Sci Adv*, 2021, **7**, eabd8523 8521.
19. Yu-Lun Chang, Ya-Fan Lin, Wan-Jung Chuang, Chai-Lin Kao, Manmath Narwane, Hsing-Yin Chen, M. Y. Chiang and S. C. N. Hsu, *Dalton Trans*, 2018, **47**, 5335-5341.
20. G. Cioncoloni, I. Roger, P. S. Wheatley, C. Wilson, R. E. Morris, S. Sproules and M. D. Symes, *ACS Catal*, 2018, **8**, 5070–5084.
21. I. Roger, C. Wilson, H. M. Senn, S. Sproules and M. D. Symes, *R Soc Open Sci*, 2017, **4**, 170593.
22. G. B. Wijeratne, M. Bhadra, M. A. Siegler and K. D. Karlin, *J. Am. Chem. Soc.*, 2019, **141**, 17962-17967.
23. P. Huang, Y. Yan, A. Banerjee, L. Lefferts, B. Wang and J. A. F. Albanese, *J Catal*, 2022, **413**, 252-263.
24. S. C. N. Hsu, Y.-L. Chang, W.-J. Chuang, H.-Y. Chen, I.-J. Lin, M. Y. Chiang, C.-L. Kao and H.-Y. Chen, *Inorg Chem*, 2012, **51**, 9297-9308.
25. P. Manikandan, K. R. J. Thomas and P. T. Manoharan, *J Chem Soc, Dalton Trans*, 2000, DOI: 10.1039/b002289f., 2779-2785
26. S. Jayantya, G. K. Prasad, B. Sreedhar and T. P. Radhakrishnan, *Polymer*, 2003, **44**, 7265-7270.
27. R. C. Maji, S. Mishra, A. Bhandari, R. Singh, M. M. Olmstead and A. K. Patra, *Inorg Chem*, 2018, **57**, 1550–1561.
28. N. Lehnert, U. Cornelissen, F. Neese, T. Ono, Y. Noguchi, K.-i. Okamoto and K. Fujisawa, *Inorg Chem*, 2007, **46**, 3916-3933.
29. E. V. Kabin, V. A. Emel'yanov and S. V. Tkachev, *Russ. J. Inorg. Chem.* , 2013, **58**.
30. G. K. S. Prakash, L. Heiliger and G. A. Olah, *Inorg Chem*, 1990, **29**, 4965–4968.
31. M. Beretta, E. Bouwman, L. Casella, B. Douziech, W. L. Driessen, L. Gutierrez-Soto, E. Monzani and J. Reedijk, *Inorg Chim Acta*, 2000, **310**, 41-50.
32. E. Monzani, G. J. A. A. Koolhaas, A. Spandre, E. Leggieri, M. G. L. Casella, G. Nardin, L. Randaccio, M. Fontani, P. Zanello and J. Reedijk, *J Biol Inorg Chem*, 2000, **5**, 251–261.
33. T. Matsui, Y. Kitagawa, M. Okumura and Y. Shigeta, *J Phys Chem A*, 2015, **119**, 369–376.
34. M. N. C. Zarycz and C. F. Guerra, *J. Phys. Chem. Lett.* , 2018, **9**, 3720–3724.
35. K. Sagarik, S. Chaiwongwattana, V. Vchirawongkwinb and S. Prueksaaroon, *Phys. Chem. Chem. Phys.*, 2010, **12**, 918–929.
36. L. Casella, O. Carugo, M. Gullotti, S. Doldi and M. Frassoni, *Inorg Chem*, 1996, **35**, 1101–1113.

37. R. Tyburski, T. Liu, S. D. Glover and L. Hammarström, *J Am Chem Soc*, 2021, **143**, 560-576.
38. T. Liu, R. Tyburski, S. Wang, R. Fernandez-Teran, S. Ott and L. Hammarström, *J Am Chem Sci*, 2019, **141**, 17245-17259.
39. T.-Y. Cheng and R. M. Bullock, *J Am Chem Soc*, 1999, **121**, 3150–3155.
40. C. C.Carmona-Vargas, S. L. Aristizábal, M. I. Belalcázar, R. F.D'Vries and M. N.Chaur, *Inorg Chim Acta*, 2019, **487**, 275-280.
41. R. C. Maji, S. K. Barman, S. Roy, S. K. Chatterjee, F. L. Bowles, M. M. Olmstead and A. K. Patra, *Inorg Chem*, 2013, **52**, 11084–11095.
42. A. C. Merkle and N. Lehnert, *Dalton Trans*, 2012, **41**, 3355-3368
43. C. E. Ruggiero, S. M. Carrier and W. B. Tolman, *Angew Chem Int Ed*, 1994, **33**, 895-897.
44. M. Kujime, C. Izumi, M. Tomura, M. Hada and H. Fujii, *J Am Chem Soc*, 2008, **130**, 6088-6098.
45. J. G. Woollard-Shore, J. P. Holland, M. W. Jones and J. R. Dilworth, *Dalton Trans*, 2010, **39**, 1576-1585.
46. A. J. Timmons and M. D. Symes, *Chem Soc Rev*, 2015, **44**, 6708-6722
47. T. F. W. Daisuke Sasaki, Robert R. Eady, Richard C. Garratt, Svetlana V. Antonyuk, S. Samar Hasnain, *The FEBS J*, 2020, **288**, 262-280.
48. N. G. H. Leferink, S. V. Antonyuk, J. A. Houwman, N. S. Scrutton, R. R. Eady and S. S. Hasnain, *Nat Commun*, 2014, **5**, 4395.
49. Y. Fukuda, H. Koteishi, R. Yoneda, T. Tamada, H. Takami, T. Inoue and M. Nojiri, *Biochim Biophys Acta*, 2014, **1837**, 396-405.
50. J. A. Halfen and W. B. Tolman, *J Am Chem Soc*, 1994, **116**, 5475–5476.
51. C.-S. Chen and W.-Y. Yeh, *Chem Commun*, 2010, **46**, 3098-3100.
52. W.-J. Chuang, I.-J. Lin, H.-Y. Chen, Y.-L. Chang and S. C. N. Hsu, *Inorg Chem*, 2010, **49**, 5377–5384.
53. Tobias M. Hedison, Rajesh T. Shenoy, Andreea I. Iorgu, Derren J. Heyes, Karl Fisher, Gareth S. A. Wright, Sam Hay, Robert R. Eady, Svetlana V. Antonyuk, S. S. Hasnain and N. S. Scrutton, *ACS Catal*, 2019, **9**, 6087-6099.
54. N. G. H. Leferink, C. Han, S. V. Antonyuk, D. J. Heyes, S. E. J. Rigby, M. A. Hough, R. R. Eady, N. S. Scrutton and S. S. Hasnain, *Biochemistry*, 2011, **50**, 4121–4131.
55. S. Brenner, D. J. Heyes, S. Hay, M. A. Hough, R. R. Eady, S. S. Hasnain and N. S. Scrutton, *J. Biol. Chem.*, 2009, **284**, 25973-25983.